Volume 8
Number 4
28 January 2020
Pages 1491–2150

Journal of Materials Chemistry A

Materials for energy and sustainability

rsc.li/materials-a

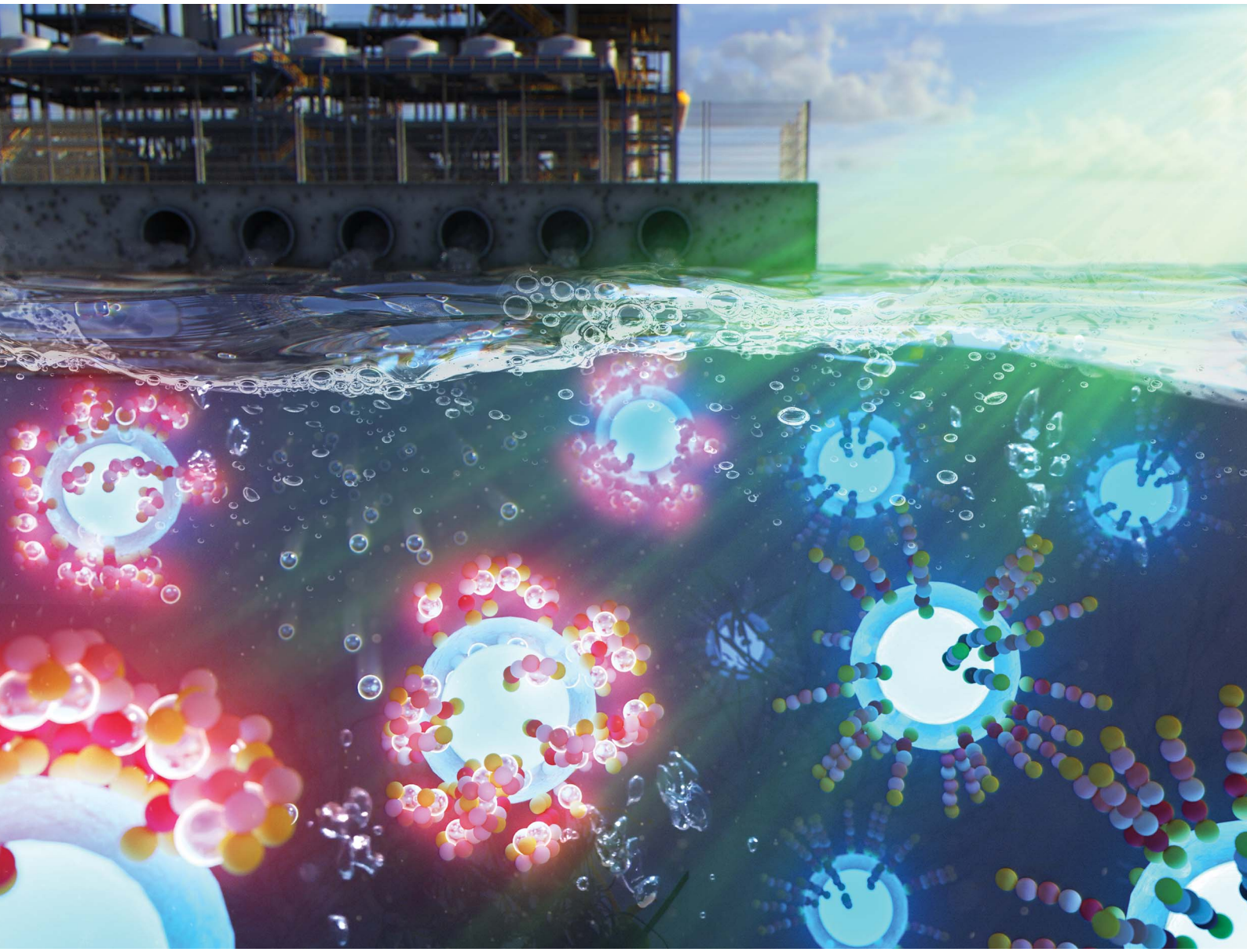

ISSN 2050-7488

ROYAL SOCIETY OF CHEMISTRY

PAPER

Hyoung-il Kim, Oh Seok Kwon *et al.*
Single-photon-driven up-/down-conversion nanohybrids for *in vivo* mercury detection and real-time tracking

Journal of Materials Chemistry A

ROYAL SOCIETY OF CHEMISTRY

PAPER

View Article Online
View Journal | View Issue

Cite this: *J. Mater. Chem. A*, 2020, **8**, 1668

Single-photon-driven up-/down-conversion nanohybrids for *in vivo* mercury detection and real-time tracking†

Sung Eun Seo,‡[ab] Chul Soon Park,‡[a] Seon Joo Park,[a] Kyung Ho Kim,[a] Jiyeon Lee,[a] Jinyeong Kim,[a] Sang Hun Lee,[c] Hyun Seok Song,[d] Tai Hwan Ha,[a] Jae-Hyuk Kim,[e] Hee Won Yim,[b] Hyoung-il Kim *[b] and Oh Seok Kwon *[af]

A multifunctional assay with up-/down-conversion (UC/DC) nanohybrids which enables the detection and real-time tracking of hazardous molecules has been developed for use in the field of photoluminescence (PL) point-of-care testing due to its cost and convenience. In particular, innovative approaches such as dual or multimodal imaging and detection under only a single-photon pulse system are highly difficult owing to the issues of device simplification and miniaturization. In this work, we first demonstrated single-photon-driven UC/DC dual-modal PL nanohybrids and showed their high performance in *in vivo* mercury detection and real-time tracking in a mussel simultaneously. Specifically, UC/DC nanohybrids capable of being stimulated by a single photon were presented *via* a facile and versatile strategy by combining DC fluorophores for heavy metal ion screening with triplet–triplet annihilation upconversion (TTA-UC) nanocapsules for real-time tracking. By adopting the advantages of the structural transformation of DC fluorophores and highly stable TTA-UC nanocapsules, the outstanding monitoring performance of a standard heavy metal ion (*i.e.* Hg^{2+}) was achieved by a dual-modal PL assay with nanohybrids, exhibiting ultra-sensitivity (under 1 nM) and high-selectivity. Interestingly, their application in the real world was also remarkable in screening and tracking of mercury in mussels. This single-photon-driven UC/DC convergence system will provide powerful analytical methodologies for target detection and real-time tracking *in vivo* and will attract widespread attention from researchers in the fields of PL nanomaterials and fluorophores.

Received 3rd October 2019
Accepted 3rd December 2019

DOI: 10.1039/c9ta10921h

rsc.li/materials-a

Introduction

Developing photoluminescent (PL) nanomaterials that enable the detection and real-time tracking of hazardous molecules with a high fatality rate is a significant task to guard human health. Many researchers have developed excellent imaging agents for the real-time tracking of such hazardous molecules due to their biological accumulation and toxicity,[1–4] as well as high-performance sensing materials to identify the presence of target molecules *in vitro* or *in vivo*. Recently, up/downconversion (UC/DC) PL nanomaterials for dual-modal cell imaging were successfully reported using nanocomposites[5] and carbon quantum dots,[6] opening up a new class of fluorescent labels for multiplexed biological imaging with a single-photon system. Conventional PL nanomaterials occasionally generate false positive results and side effects *in vitro*/*in vivo* due to their low selectivity. Moreover, there is no real-time tracking function in PL nanomaterials because a tracking system requires more labels and additional excitation sources. Although PL nanomaterials enable the detection of trace amounts of target molecules along with imaging in cells or organs, these systems have limitations in selectivity and tracking information. In addition, nanomaterials with PL properties are required to emit UC/DC luminescence under a single-photon pulse, and each emission wavelength must be far enough apart to prevent spectral overlap. Therefore, to overcome these limitations, a new methodology such as simultaneous detection and tracking is needed.

[a]*Infectious Disease Research Center, Korea Research Institute of Bioscience and Biotechnology (KRIBB), 125 Gwahak-ro, Yuseong-gu, Daejeon 34141, South Korea. E-mail: oskwon7799@gmail.com*

[b]*Department of Civil and Environmental Engineering, Yonsei University, Seoul 03722, South Korea. E-mail: hi.kim@yonsei.ac.kr*

[c]*Department of Bioengineering, University of California Berkeley, CA 94720, USA*

[d]*Sensor System Research Center, Korea Institute of Science and Technology, Seoul 02792, Republic of Korea*

[e]*Department of Chemical and Environmental Engineering, Pusan National University, 46241 Busan, Korea*

[f]*Nanobiotechnology and Bioinformatics (Major), University of Science & Technology (UST), 125 Gwahak-ro, Yuseong-gu, Daejeon, 34141, South Korea*

† Electronic supplementary information (ESI) available. See DOI: 10.1039/c9ta10921h

‡ S. E. Seo and C. S. Park contributed equally to this work.

Compared to conventional DC, which is a conversion process from photons with low frequency to photons with higher frequency, upconversion (UC) such as organic chromophore dye pair based triplet–triplet annihilation assisted upconversion provides a potential imaging strategy owing to its effective tissue penetration with excitation in the visible light range, low power irradiation and lack of optical noise from background autofluorescence.[7–11,43] Many UC materials, consisting of rare earth ion (lanthanide ion)-doped inorganic crystals, have been synthesized for bioimaging[12,13] and also for therapy applications,[14,15] but they suffer from inherent problems arising from their requirement for extremely high-power excitation and poor quantum yield (QY).[44] These limitations have accelerated the development of an alternative UC strategy, particularly an organic chromophore-based system: triplet–triplet annihilation (TTA)-based UC. However, organic TTA-UC molecules also have weak properties toward solvents, especially water, because of their quenching effect on upconverted photons.[45] In our previous work, we demonstrated TTA-UC nanocapsules produced with a microemulsion system and confirmed their high QYs with a long wavelength range in the aqueous phase.[16–18] Moreover, TTA-UC nanocapsules enabled dual-color emissive cancer cell imaging *in vitro* and *in vivo* under only a single-photon pulse.[17] Therefore, the application of TTA-UC nanocapsules remains a challenge.

Turn-on fluorescent sensing, which is a DC method, with reactive chemical probes, fluorophores, is a suitable tool for the detection of disease molecules and hazardous compounds because the chromophore pair has a high selectivity and sensitivity for small molecules, especially heavy metal ions in mixtures.[19–29] Fluorophores with various interaction sites have been designed for high-efficiency turn-on/off intensity and have also been developed based on receptor–analyte noncovalent interactions, such as electrostatic and donor–acceptor interactions, resulting in high-performance metal-coordination binding readouts in the aqueous phase. Therefore, the use of fluorophores for sensing analytes provides a creative methodology for the detection and tracking of heavy metal ions by DC PL.

In this work, we first demonstrated single-photon-driven UC/DC nanohybrids for environmental monitoring and real-time *in vivo* tracking in a mussel. In particular, the core part of the TTA-UC nanocapsules is consisted of a TTA-UC liquid oil-phase containing two different organic chromophores, which was surrounded by a rigid silica shell. The surface of the nanocapsules was functionalized with turn-on fluorophores, namely, rhodamine hydrazide (Rho-Hz). The TTA-UC phase in the nanocapsules prepared by using a microemulsion system was used as a reagent for their real-time tracking, while DC fluorophores conjugated on the nanocapsule surface detected various concentrations of standard mercury samples. The most important advantage of this single-photon-driven UC/DC system is that there is no need to consider the possibility of uneven dispersion of the target-detecting probe over the sample which causes a false negative signal. The limit of detection (LOD) of the nanohybrids was *ca.* 1 nM. Moreover, the dual-modal PL nanohybrids showed attractive *in vivo* mercury detection and real-time tracking in a mussel under a single-photon pulse.

Experimental section

Materials

Tetrahydrofuran (THF, >99.9%), oleic acid (OA, ≥99.0%), (3-aminopropyl)triethoxysilane (APTES, 99%), (3-aminopropyl)trimethoxysilane (APTMS, 97%), tetraethyl orthosilicate (TEOS, 99.999%), 9,10-diphenylanthracene (DPA, 97%), mercury(II) perchlorate hydrate (98%), glyoxal solution (40 wt%), rhodamine B (95%), lead(II) perchlorate trihydrate, nickel(II) perchlorate hexahydrate, magnesium perchlorate hexahydrate, zinc perchlorate hexahydrate, lithium perchlorate, iron(II) perchlorate hydrate, cobalt(II) perchlorate hexahydrate, cadmium perchlorate hydrate, silver perchlorate hydrate and hydrazine hydrate were purchased from Sigma-Aldrich and PtOEP from Frontier Scientific. All reagents and solvents were used as received without further treatment. A stock solution of PtOEP (1.8 mM) and DPA (60.53 mM) in THF was prepared and stored in the dark.

Preparation of oil-phase TTA-UC

A chromophore pair, the sensitizer (PtOEP, 0.0018 M) and acceptor (DPA, 0.06053 M), was dissolved in THF separately to prepare core phases of TTA-UC nanocapsules. The stock solutions of two chromophore dyes, PtOEP and DPA, were added into oleic acid with different volumes (PtOEP: 50 μL and DPA: 600 μL) and vortexed for a few seconds to mix evenly. The oil-phase TTA-UC was left in a 70 °C oven to evaporate residual THF for 24 h. The solution was stored in the dark after evaporation to prevent the quenching effect of the dye under a fluorescent lamp.

Synthesis of the rhodamine-hydrazine (Rho-Hz) probe

Into a round bottom flask, absolute ethanol (50 mL) and rhodamine B (1.2 g, 2.5 mmol) were added and stirred vigorously at room temperature. Hydrazine hydrate (3 mL) was added after gradually rising the temperature of the rhodamine B solution to 100 °C and stirred under reflux for 6 hours. The opaque solution slowly changed to transparent when the reaction ended. The resultant solvent was evaporated thoroughly. The final product was washed using filter paper to obtain pure Rho-Hz.[42]

Synthesis of TTA-UC nanocapsules

The TTA-UC nanocapsules were fabricated using a microemulsion method. 500 μL of oil-phase TTA-UC solution was added into 28.8 mL distilled water drop by drop under vigorous stirring to form a micelle suspension. After stirring for 1 hour, the oil solution containing two different chromophores was sonicated for 15 min. After dispersion of the oil-phase TTA-UC solution, 390 μL of APTES was added and soon after 2.49 mL of TEOS were added dropwise. The solution containing upconversion nanocapsules was aged overnight in a 55 °C oven for curing the nanocapsules. The synthesized nanocapsules were washed with distilled water (4000 rpm, 3 min). After washing, 30 mL of

solution was stirred with 0.98 mL APTMS for 24 h at 100 rpm in a hot water bath. Through this process, the surface of the TTA-UC nanocapsules was functionalized with amine groups for a further linker conjugation process. The final product was obtained after several washing steps with distilled water.

Chemical probe attachment on TTA-UC nanocapsules

The surface of TTA-UC nanocapsules was modified with 40 wt% glyoxal solution after the functionalization with the amine group. Specifically, first of all, 40 wt% glyoxal solution was diluted to 5 wt% with distilled water, making the total volume to 50 mL. And 3 mL of nanocapsule solution was added into 50 mL of glyoxal solution and they are placed under vigorous stirring for 1 h. The resulting mixture was washed several times with distilled water to remove the residual glyoxal solution that didn't react with the nanocapsules. Next, the nanocapsules the surface of which are functionalized with glyoxal were injected into 11 μM rhodamine-Hz solution under vigorous stirring and kept under stirring for 3 h in a hot water bath. The aldehyde functionalized nanocapsules were covalently conjugated with the amine groups of the as-synthesized Rho-Hz.

Sample preparation of mercuric ions

The detection of mercuric ion experiment was conducted with standard material before conducting with the real sample. Mercury(II) perchlorate hydrate was prepared by serial dilution with distilled water from 10^{-9} M to 10^{-4} M. The prepared TTA-UC nanocapsules were contained in a quartz cuvette. The diluted mercury solutions (100 μL) were added into the cuvette. The added mercury reacts with Rho-Hz which is conjugated on the surface of the TTA-UC nanocapsules. Under a 532 nm light source, from the TTA-UC nanocapsules, there were two light emissions: one is up-converted emission from the nanocapsules and the other is the down-converted emission from the surface of the TTA-UC nanocapsules which indicates the reaction of mercury with Rho-Hz.

Characterization of nanocapsules

The fluorescence of the TTA-UC nanocapsules was measured in a quartz cuvette cell using a fluorescence spectrometer system (Model SR810 DSP Lock-in Amplifier and monochromator with a 3502 optical chopper; New Focus) under 532 nm wavelength excitation. The emitted fluorescence light entered the monochromator through a 500 nm short-pass filter to block excitation light. Transmission electron microscopy (TEM) images were taken to visualize the prepared nanostructure and the morphology with a Tecnai G2 F30. Scanning electronic microscopy (SEM) images were recorded on a Hitachi SU8230 microscope. The absorbance was analyzed by using a UV/VIS spectrometer (Beckman Coulter, DU800).

Results and discussion

Synthesis and characterization of TTA-UC nanocapsules with fluorophores[16,17]

We prepared highly monodisperse dual-conversion fluorescent nanohybrids composed of materials with completely opposite emission behaviors under a single-photon pulse. Initially, to enable a real-time tracking function by UC, TTA-UC nanocapsules were prepared by benchmarking a micro-emulsion method based on our previous reports. The synthesis proceeded through the dissolution of a chromophore pair in tetrahydrofuran: platinum octaethylporphyrin (PtOEP) as a sensitizer and 9,10-diphenylanthracene (DPA) as an acceptor. The chromophore dye pair was dissolved and emulsified with oleic acid (OA) as a surfactant to form a spherical micro-emulsion template (Fig. 1a). The dispersed micro-emulsion capsules decreased in size to the nanoscale after adding (3-aminopropyl)-triethoxysilane (APTES) owing to their charge interaction, which can be confirmed by the color change from a transparent solution to a suspension with an opaque white color (Fig. 1b). Upon adding tetraethyl orthosilicate (TEOS), silicon dioxide was formed on the surface of the nano-sized emulsion capsules, and then TTA-UC nanocapsules with a rigid silica shell were synthesized after an appropriate annealing process (Fig. 1c). To facilitate the bioconjugation of the synthesized TTA-UC nanocapsules, (3-aminopropyl)-trimethoxysilane (APTMS) was applied to form amine functional groups on the surface of the TTA-UC nanocapsules (Fig. 1d). The surface modification of the TTA-UC nanocapsules provides more active sites for bio/chemical probe conjugation.

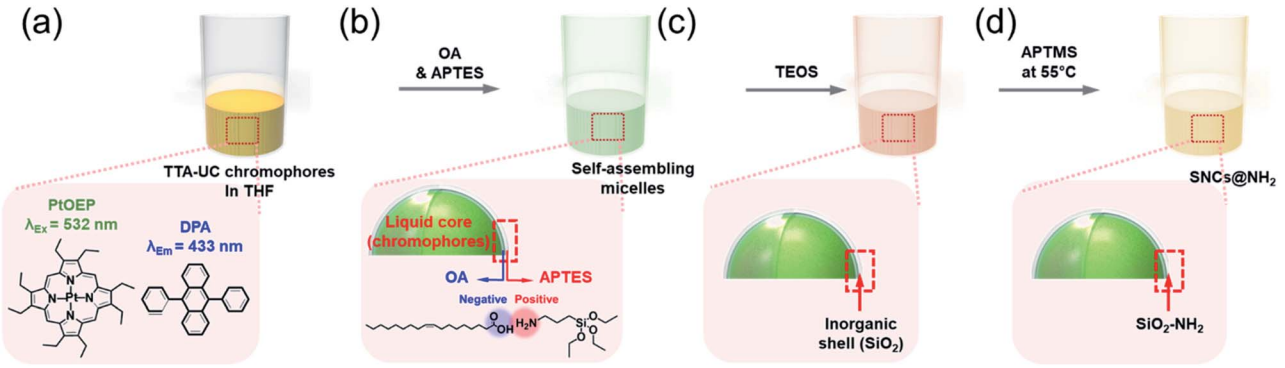

Fig. 1 Schematic illustration of the TTA-UC nanocapsule assembly procedure (a) based on the micro-emulsion method. (b and c) Formation of a silica shell around the micelles and (d) surface modification of TTA-UC nanocapsules with amine functional groups.[16]

The TTA-UC nanocapsules have attractive advantages, such as water-dispersible hydrophilic silica shells, facile surface modification and high-efficiency QYs, owing to their protection from singlet oxygen by unsaturated double bonds in the OA backbone, enabling biorelated applications.

In the core of the TTA-UC nanocapsules, a sensitizer and acceptor chromophore pair was introduced for efficient TTA-UC irradiation because their mechanism is based on Dexter energy transfer (Fig. 2a).[30] The ground state sensitizer (SENS) can be excited with a single-photon pulse system ($\lambda_{Ex} = 532$ nm), which is expressed as SENS* in Fig. 2a, and the energy of the excited sensitizer (SENS*) is transferred to the ground-state acceptor. This energy transfer is called triplet–triplet energy transfer (TTET). Two excited acceptors (ACC*) are impacted and emit upconverted light; then, the excited sensitizers return to the ground state.[31] With this anti-Stokes shift, a photon with low energy (*ca.* 2.3 eV, a green color) is converted to a photon with higher energy (*ca.* 2.9 eV, a blue color), which we call upconversion (Fig. 2b). The characteristics of the chromophore dyes were analyzed with absorption and PL emission spectroscopy (Fig. 2c). The absorption peak of PtOEP showed the characteristics of a porphyrin: a strong Soret band (<400 nm) is accompanied by weaker Q-band absorption (501 and 535 nm).[32] As shown in the graph, the maximum PL of PtOEP in tetrahydrofuran (THF) solution is located at 641 nm, and DPA has an excitation wavelength varying from 400 to 500 nm. The UC system was observed with the naked eye in the OA solution with chromophore dye pairs (Fig. 2d). As control experiments, samples with each chromophore dye and the chromophore dye pair were prepared in the same cuvette with OA solution. The control samples showed bright DC light from each chromophore dye, while the coexisting pair sample displayed UC light under a single-photon pulse. The photon is transformed efficiently from green (2.33 eV) into blue (2.9 eV) emission because the chromophore pair dissolved OA showed an absorption peak ranging from 500 nm to 550 nm (Fig. 2e). The UC emission intensity increased proportionally depending on the power of the laser (532 nm) (Fig. 2f). The power range of the irradiated light varies from 350 mW cm^{-2} to 1177 mW cm^{-2}. The QY of the upconverted light was measured using an equation and compared with that of rhodamine 6G as a reference (Fig. 2g and S3†). The maximal QY of the TTA-UC nanocapsules was calculated to be *ca.* 2%, and the results of their photostability test, in which a temporary laser was used until the fluorescence of the

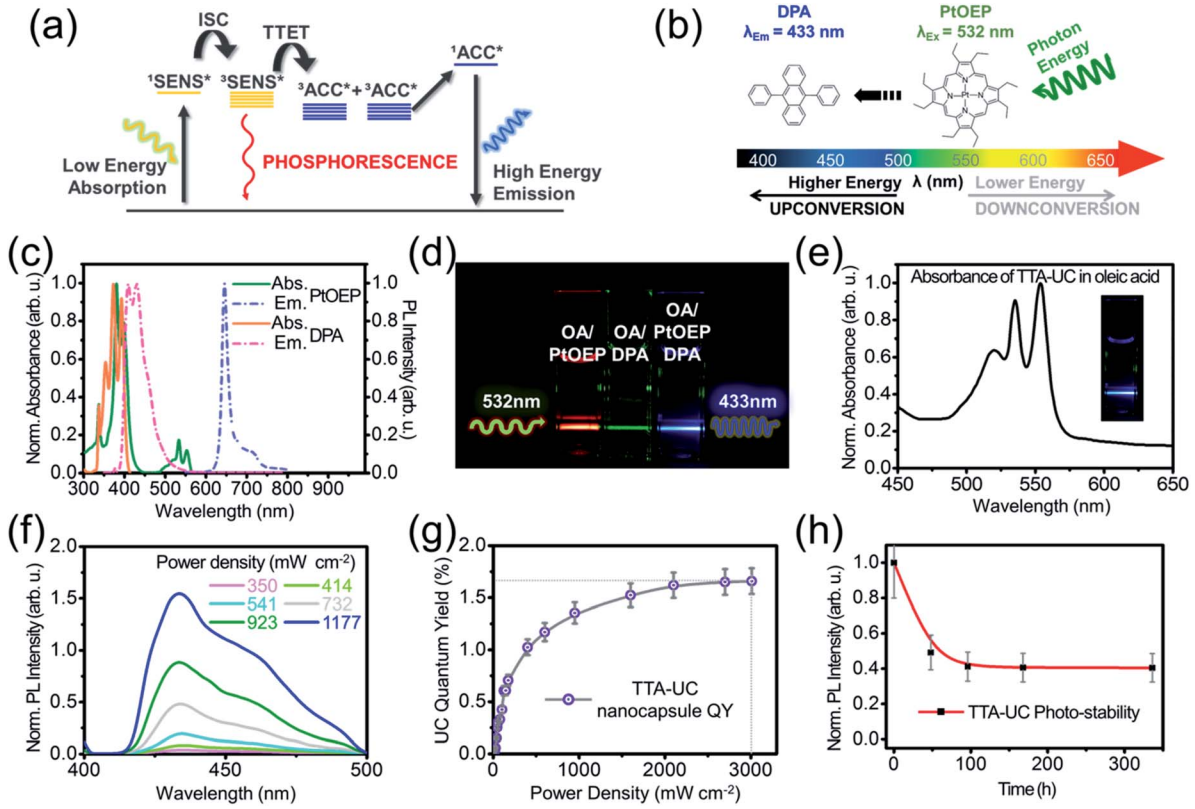

Fig. 2 (a) UC mechanism that occurs in the core of the TTA-UC nanocapsules (ISC: Intersystem crossing, TTET: Triplet–triplet energy transfer, SENS: sensitizer, and ACC: acceptor). (b) Chemical structures of PtOEP and DPA with a light spectrum from the UV to the IR range (400–650 nm). (c) Normalized absorption (solid line) and emission (dashed line) spectra of PtOEP and DPA: [PtOEP] = 0.0040 mM and [DPA] = 0.072 mM. (d) Photographs of oil solutions in cuvette cells containing sensitizer only (left), acceptor only (middle), or both sensitizer and acceptor (right). (e) The absorbance graph of the chromophore dye pair dissolved OA solution. The inset shows a photograph of the converted emission through the TTA-UC process under a single-photon pulse. (f) Emission variations of TTA-UC as a function of incident light power density (350, 414, 541, 732, 923 and 1177 mW cm^{-2}) under excitation at 532 nm. (g) UC QY of the PtOEP/DPA system in OA as a function of laser power density. (h) Photostability test of the chromophore pair dissolved oil solution under temporary laser power density (663 mW cm^{-2}).

chromophore dye pair dissolved oil solution is weakened, demonstrated that the fluorescence remained for more than 300 h. The concentration of the nanocapsule was more than 0.06 wt%.[18] Low concentration of the TTA-UC nanocapsules induces less fluorescence. And the upconverted emission from the TTA-UC nanocapsules lasted for up to 10.6 h under a continuous 353 mW cm^{-2} laser power intensity, which was varied from 353 mW cm^{-2} to 663 mW cm^{-2} (Fig. 2h and S4†).

To measure the physical and chemical properties of the TTA-UC nanocapsules, such as their morphology, optical performance, and UC efficiency, scanning electron microscopy (SEM) and transmission electron microscopy (TEM) and photostability tests were performed (Fig. 3). The TTA-UC nanocapsules had a uniform morphology and were monodisperse in the liquid phase, as observed by SEM (Fig. 3a). Size distribution analysis was carried out with the ImageJ program (Fig. 3a inset). The particle size distribution graph displayed that the TTA-UC nanocapsules exhibit an average size of approximately 200 nm. As revealed by TEM images, nanocapsules with the chromophore pair in the solution in their inner section were clearly observed, and the surface was composed of a rigid silica shell with *ca.* 23 nm in shell thickness (Fig. 3b). The TTA-UC nanocapsule image shows that the core contains a liquid chromophore pair and that the surface is enclosed with a rigid silica shell (Fig. 3b inset).[33,34]

Upon excitation at 532 nm (*ca.* 2.3 eV, green light) with various power intensities, including 238 mW cm^{-2}, 398 mW, 557 mW cm^{-2}, 876 mW cm^{-2}, and 1194 mW cm^{-2}, the PL emission peak of the TTA-UC nanocapsules at a wavelength of 433 nm showed variable intensity, which indicates a TTA-UC process (Fig. 3c). The intensity of the emitted light was highly dependent on the power density of the incident single-photon source at 532 nm. The greater the energy irradiated on the nanocapsules, the greater the number of photons transferred to a higher energy state and emitted from the TTA-UC nanocapsules. The upconverted light intensity peak at approximately 433 nm was plotted and showed a quadratic increase instead of a linear increment, which is a primary characteristic of the UC mechanism (Fig. 3d). In addition, a photostability test of the TTA-UC nanocapsules was carried out under the same conditions as the prior experiment with TTA-UC OA solution (Fig. 3e). The nanocapsules showed ultrastable photostability for more than 3 h toward a high irradiation power of 1194 mW cm^{-2}, which is used with high-performance PL probes.

The location where mercury is accumulated in water has been observed by the quenching of fluorophores. However, those methods have a critical limitation in accuracy because of high signal-to-noise ratios. To overcome this hurdle, an advanced detection approach with great selectivity and sensitivity, namely, the synthesis of Rho-Hz reported in a previous paper, was introduced for monitoring the location and amount of mercury at the same time under a single-photon pulse.

Rho-Hz, an attractive fluorophore for metal ion detection in aqueous solution, was synthesized *via* a one-step reaction of rhodamine B with hydrazine hydrate in ethanol under reflux conditions (Fig. 4a). The crude product was purified by silica column chromatography and recrystallized from ether/*n*-hexane. Specifically, Rho-Hz was characterized with NMR and mass spectrometry (see ESI Fig. S6†). In addition, the N-terminus of the spirolactam of Rho-Hz was able to link with a variety of aldehydes for the selective detection of a metal ion. Among the aldehydes, the use of glyoxal allows selective binding

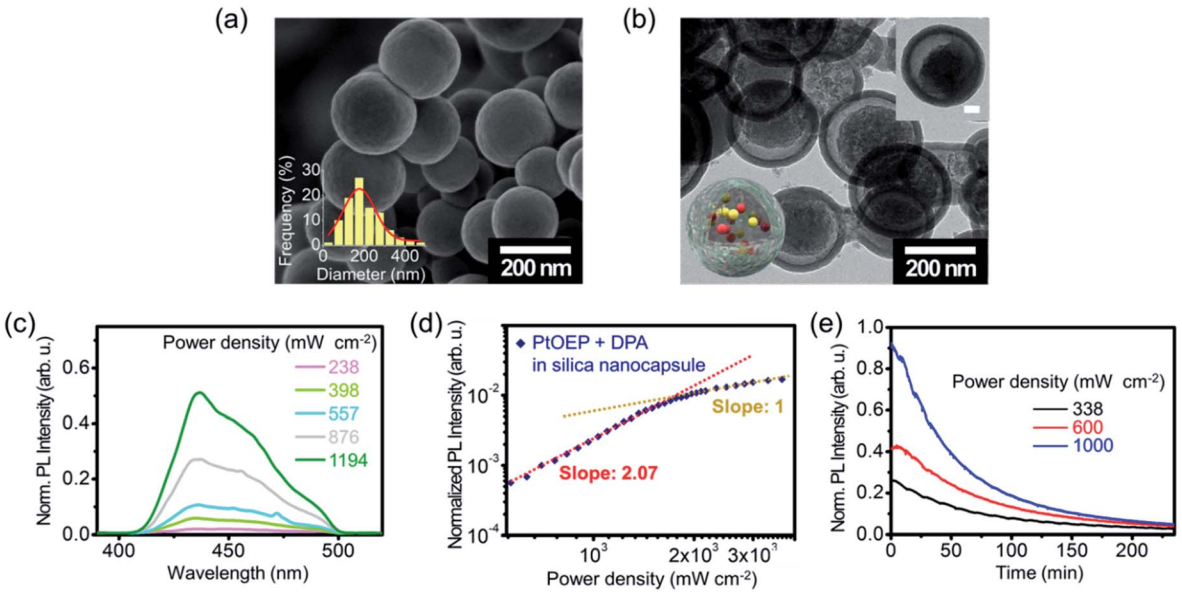

Fig. 3 (a) SEM image and (b) TEM image of TTA-UC nanocapsules: each inset shows size distribution diagrams of the TTA-UC nanocapsules and illustration of the nanocapsules with the liquid chromophore pairs. Inset scale bar = 50 nm. (c) The emission intensity of TTA-UC nanocapsules as a function of incident single-photon sources (238, 398, 557, 876, and 1194 mW cm^{-2}) under irradiation at 532 nm. (d) log–log graph of the TTA-UC intensity. (e) Photostability test of the TTA-UC nanocapsules under different incident laser power densities (338, 600 and 1000 mW cm^{-2}). A PL intensity of 20% was reached after 2 h.

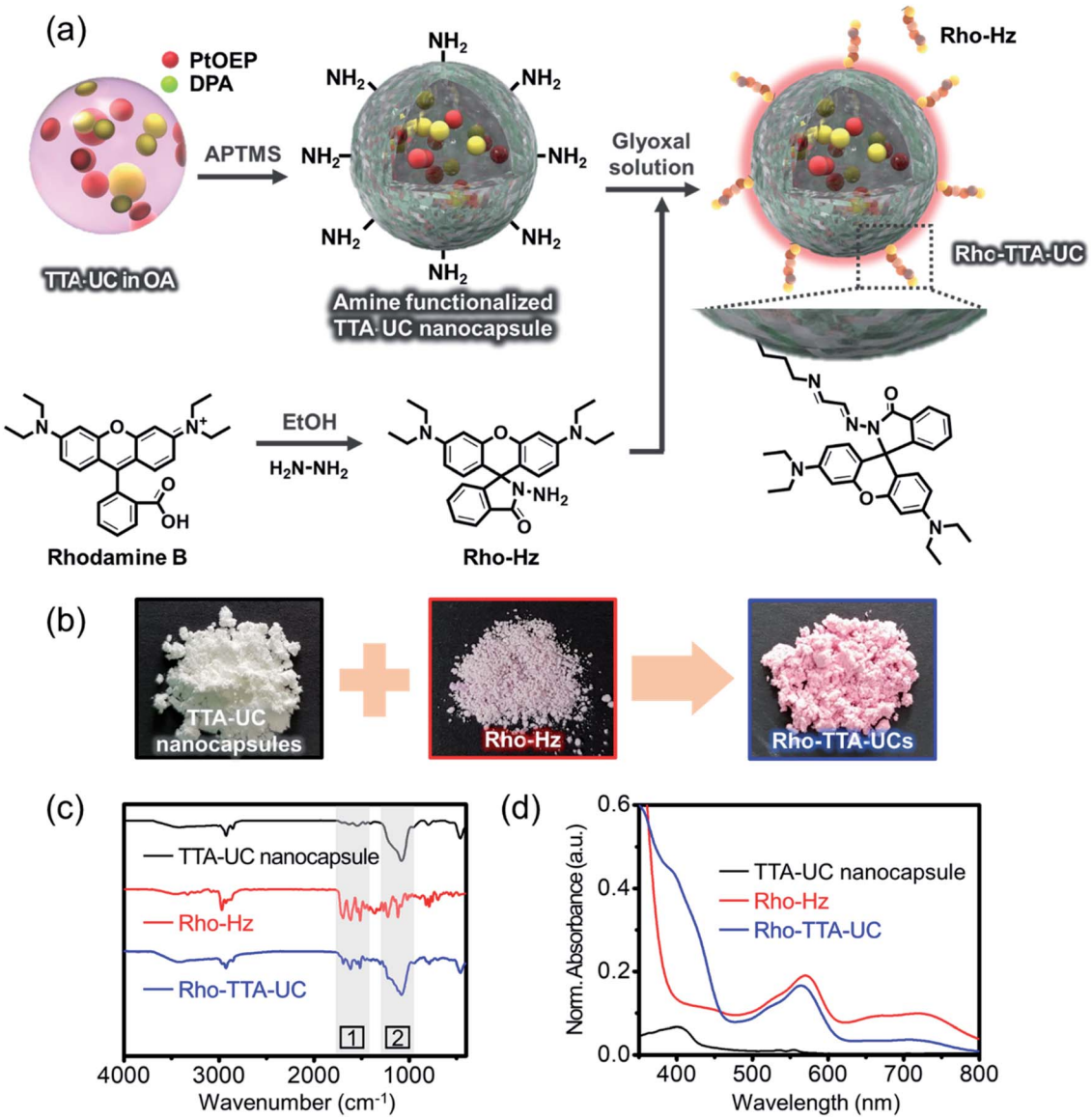

Fig. 4 (a) Fabrication procedure of Rho-Hz-conjugated TTA-UC nanocapsules *via* surface functionalization. (b) Pictures showing each color change of the TTA-UC nanocapsules, Rho-Hz and Rho-TTA-UNs. (c) FT-IR spectra confirming the conjugation of Rho-Hz: amine-functionalized TTA-UC nanocapsules (black solid line), Rho-Hz (red solid line), and Rho-TTA-UNs (blue solid line). (d) Absorbance data for the TTA-UC nanocapsules, Rho-Hz and Rho-TTA-UNs.

with mercury ions.[35–38] Various rhodamine-B derivatives can bind to each metal ion specifically by a spirolactam ring-opening process, such as Cu^{2+}, Pb^{2+}, Zn^{2+}, Fe^{3+} and Hg^{2+}, depending on the structure of chelating moiety of the rhodamine.[39] Also, according to hard and soft acids and bases theory (HSAB theory), the selective binding affinity is decided by the acidity of the metal ion and chelating part of the rhodamine derivative.[40] The mercury ion is one of the soft acids, and the carbonyl group of the Rho-Hz is a soft base. The mercury ion showed strong affinity to the chelating moiety of Rho-Hz. Therefore, the introduction of Rho-Hz onto TTA-UC nanocapsules provides highly sensitive and selective mercury detection by a turn-on process.

Surface modification of the TTA-UC nanocapsules enables stable conjugation with chemical and biological moieties (Fig. 4b). For the selective detection of mercury, the surface of the TTA-UC nanocapsules was functionalized with amine groups, and Rho-Hz, which interacts with mercury ions, was incorporated onto their surface by adding a conjugation reagent (glyoxal solution). Specifically, Rho-Hz dissolved in an organic solution was added to glyoxal-conjugated TTA-UC nanocapsules. The presence of Rho-Hz on the surface of the TTA-UC nanocapsules (Rho-TTA-UNs) was confirmed by Fourier transform infrared (FT-IR) spectroscopy (Fig. 4c). The presence of amine functional groups on TTA-UC nanocapsules and Rho-Hz is indicated by FT-IR spectroscopy which give rise to peaks at 3300–3500 cm^{-1}.[47] Absorbance spectra of the reference

materials, such as the bare TTA-UC nanocapsules and raw Rho-Hz by itself, were compared to that of the Rho-TTA-UN nanohybrids (Fig. 4d). The bare TTA-UC nanocapsules had no significant peaks corresponding to Rho-Hz in their FT-IR and absorbance spectra. By contrast, the FT-IR data for Rho-TTA-UNs showed an indicative increase in the range of 1000–1800 cm^{-1}. In addition, the spectrum presented Rho-Hz spirolactam amide carbonyl (C=O) stretching vibration at 1689 cm^{-1}.[46] And the UV-VIS spectra showed a dramatic change in the Rho-Hz-conjugated TTA-UC nanocapsule spectrum.

Overall reaction methodology of the multifunctional nanohybrids

In our research, the most attractive point of the multifunctional assay system is that up-/down-conversion photoluminescence is emitted from the mercury containing sample solution simultaneously under a single-photon source. Without the light source, the solution could not emit fluorescence (Fig. 5a). The green range of the light source was irradiated directly on sample solution that contains PL nanohybrids. In the sample solution, PL nanohybrids absorb the photon energy and upconversion photoluminescence is emitted from the core part that contains the TTA-UC chromophore dye pair (Fig. 5b). Upconverted emission enabled a signal to track the path of the PL nanohybrids in an actual sample detection experiment. Even in the absence of a target material, there is no need to concern about the false negative signal that occurs as a result of an uneven dispersion of the target-detecting probe over the sample. The opposite conversion, downconverted red emission (570 nm), only occurs when mercury ions exist in the sample (Fig. 5c). The intensity of downconverted emission can be interpreted as the amount of the target material accumulated in the sample. Under a single-photon source and single probe, by utilizing the energy conversion in the opposite direction, the location where the probe is dispersed and the amount of the target molecule that is accumulated can be monitored simultaneously (Fig. 5d). These multifunctional nanohybrids provide the benefit of effective usage of photon energy. Dual-converted emission does not interrupt the intensity or the range of wavelengths. The usage of a novel fluorescence "turn-on" detection system for the sensing of mercury ions is expanded to detect other harmful materials by simply changing the target binding ligand.

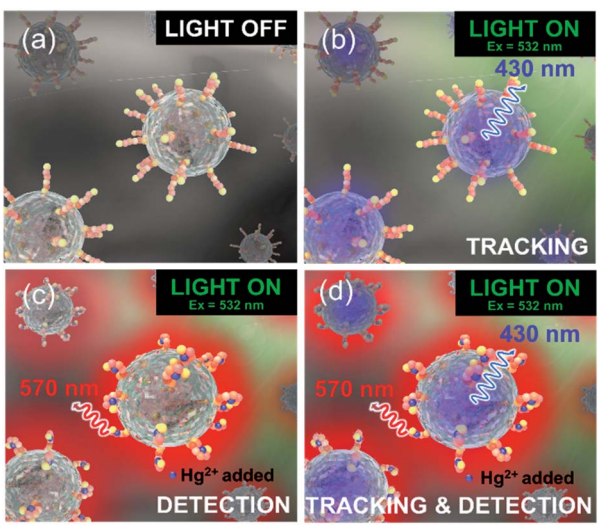

Fig. 5 Schematic illustration of the overall detection process of mercury in the sample solution. Dual converted-emission comes from the Rho-Hz conjugated TTA-UNs under a single-photon source (green laser; 532 nm). (a) Without the photon source, there is no emission from the sample solution containing the Rho-Hz conjugated TTA-UNs. (b) With a green laser as the excitation source and no mercury in the sample solution, the blue emission (430 nm) is upconverted from the core of the TTA-UNs. (c) Without the chromophore dye in the core part of the nanohybrids, in the mercury containing solution, only downconversion occurs. (d) Under irradiation of a laser, the up/downconverted emission is confirmed simultaneously. The first emission is upconverted emission from the part of TTA-UNs and the other is downconverted red emission (570 nm) that came from Rho-Hz bound on the surface of TTA-UNs which reacts with mercury. Depending on the presence of mercury in the sample, different emission can be monitored.

PL measurements of Rho-TTA-UNs for mercury detection

Rho-TTA-UNs have two different emissions at distinct wavelengths under a single-photon pulse when they interact with mercury. One is upconverted emission, which has higher energy than the irradiated light and occurs through triplet–triplet energy transfer between the chromophore dye pair inside the silica shell; the other is downconverted emission induced by the Rho-Hz-mercury interaction. Therefore, to characterize the Rho-TTA-UN system, samples with various mercury concentrations were assessed.

For high-performance mercury detection, the PL intensity of Rho-Hz in solution was measured, and Rho-Hz conjugation was optimized by varying the Rho-Hz concentration with a maximum concentration of *ca.* 11 μM. To observe the

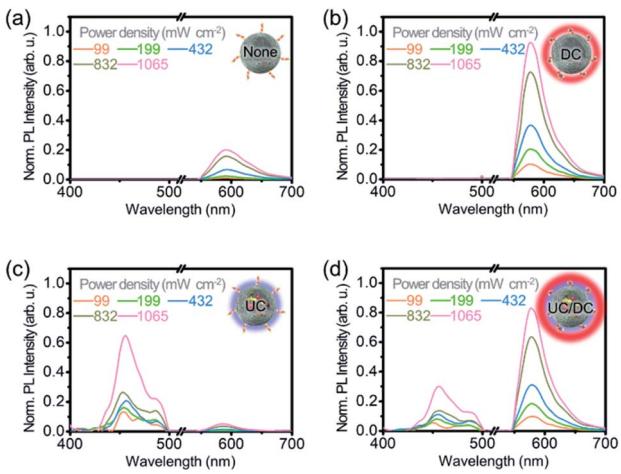

Fig. 6 Normalized fluorescence intensity using Rho-TTA-UNs for mercury detection: (a) and (b) without the chromophore dye pair and (c) and (d) with the chromophore dye pair in the inner core part of the nanocapsules. The fluorescence intensities were measured (a) and (c) without mercury ions and (b) and (d) with mercury ions. (d) Up/down-converted emission under a single-photon pulse (*ca.* 532 nm).

emissions of the Rho-TTA-UNs, several samples, such as Rho-TTA-UNs without or with the chromophore pair in the core parts of the nanocapsules, were prepared, and their reactivity with Rho-Hz and interaction with mercury were confirmed by various comparative data (Fig. 6). Rho-TTA-UNs without the chromophore pair and mercury showed no emission (Fig. 6a). By contrast, Rho-TTA-UNs without the chromophore pair exposed to a mercury solution displayed only downconverted emission from Rho-Hz owing to the Hg^{2+} chelated complex with the opened spirolactam ring of Rho-Hz (Fig. 6b). However, the Rho-TTA-UNs including the chromophore pairs showed the up- and down-converted emission for mercury detection under a single-photon pulse (Fig. 6c and d). Therefore, the Rho-TTA-UNs are suitable materials for mercury detection and real-time tracking *in vitro* and *in vivo*.

Generally, mercury ions are readily found in seafood. Among the different types of seafood, mussels are known to have strong metal ion binding properties. For this reason, mussels are commonly used as a real-world sample to monitor contamination by heavy metal ions. Knowledge of the accumulation of mercury in freshwater fish and shellfish is important because of their potential to poison people. The uptake of mercury causes a number of fatal diseases, such as Minamata disease, pulmonary edema and nephrotic

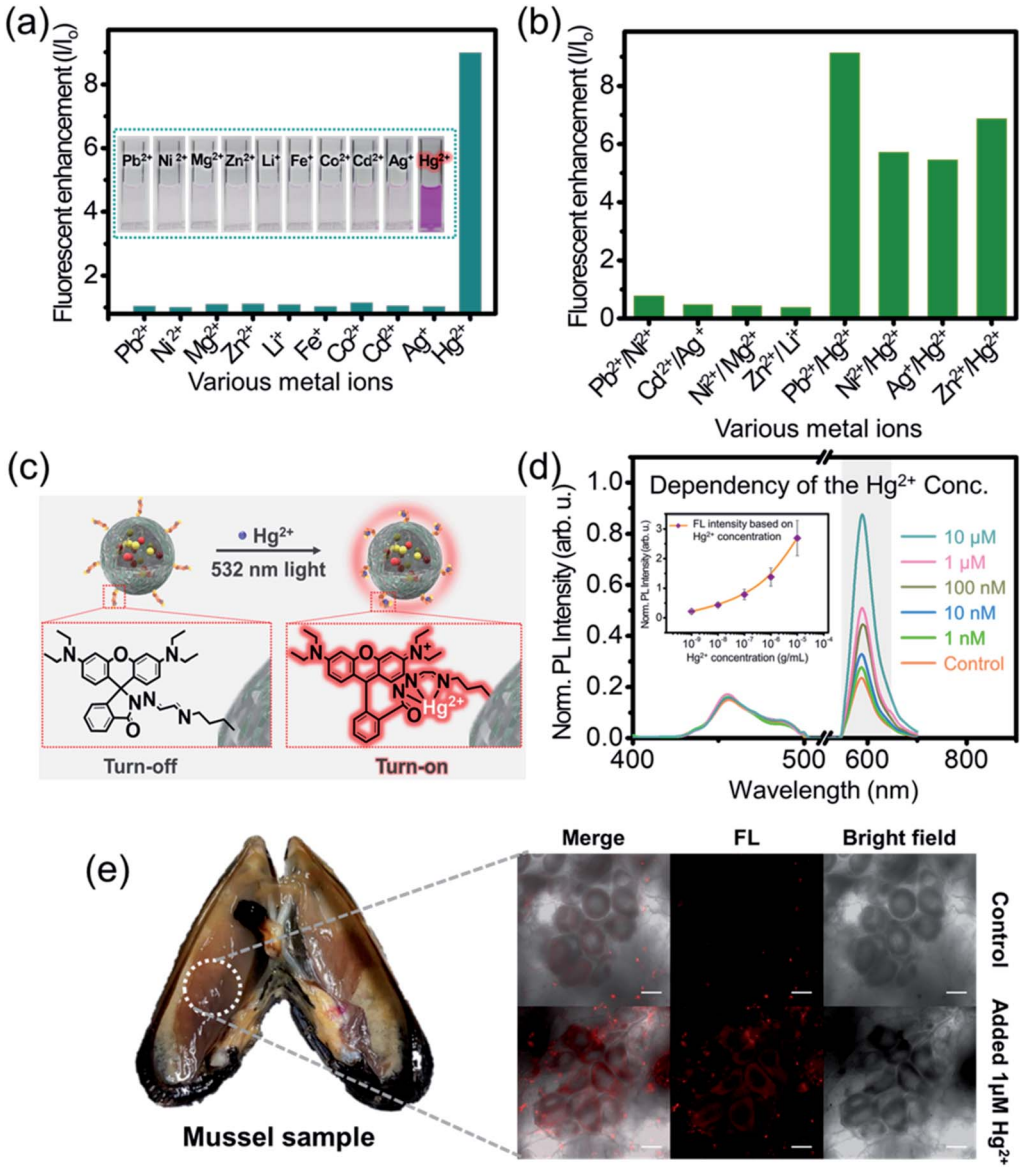

Fig. 7 (a) Selectivity test of Rho-Hz to mercury in the presence of a selection of metal ions (Ag^{+}, Zn^{2+}, Pb^{2+}, Mg^{2+}, Li^{+}, Fe^{2+}, Co^{2+}, Cd^{2+}; 1 μM each). (b) The fluorescence enhancement of Rho-Hz under various combinations of metal ions. (c) Schematic illustration of the reaction mechanism between Rho-Hz on TTA-UC nanocapsules and mercury. (d) PL intensity of the UC/DC of Rho-TTA-UNs depending on the mercury concentrations (control; 0, 1 nM, 10 nM, 100 nM, 1 μM, and 10 μM). (e) The image of the mussel sample and the circled inner part is the location of a further fluorescence image (left). Emission image of Rho-Hz after reaction between Rho-TTA-UN and mercury in a mussel (right). Inset scale bar = 40 μm.

syndrome. Therefore, precise and sensitive mercury detection is needed for human healthcare. Compared with conventional PL-based measurements for mercury ions, Rho-TTA-UNs are characterized as advanced functional nanohybrids with UC/DC capability.

To enable *in vivo* mercury detection in a mussel, Rho-TTA-UNs were prepared, and their PL intensity values were measured. First, a selectivity test with several metal ion solutions confirmed the highly specific reactivity of Rho-Hz with only the target ion, mercury, owing to its glyoxal structure (Fig. 7a). The test was done under the conditions of pH 7 diluted water solution in the presence of different species of metal ions, such as 1 μM Pb^{2+}, Ni^{2+}, Mg^{2+}, Zn^{2+}, Li^{+}, Fe^{2+}, Co^{2+}, Cd^{2+}, Ag^{+} and Hg^{2+}. Furthermore, to evaluate the possible interference of the coexisting metal ions in mercury detection, another experiment was also done with various combinations of metal ions that are contained in the cuvette (Fig. 7b). As shown in the experimental result, only mercury induced a fluorescence enhancement and other metal ions could not react with Rho-Hz. The Rho-Hz–Hg complex formation was also confirmed by conversion from colorless and non-fluorescent (spirolactam ring) to a pink color and fluorescent (ring-opened amide structure). Second, the reaction mechanism between Rho-Hz and mercury is suggested as a ring-opening-related turn-on process (Fig. 7c). As soon as mercury is added to Rho-Hz, the ring structure is opened and mercury is chelated into the chelating moiety of rhodamine. Moreover, the reaction time for the turn-on process was under *ca.* 5 s, which is suitable for point-of-care testing. In addition, the effects depending on the *in vivo* mercury concentration were characterized by PL intensity to determine the LOD (Fig. 7d). The emission wavelength from Rho-Hz is 570 nm, and the upconverted emission from the TTA-UC nanocapsules was 430 nm. As the amount of mercury increased *in vivo*, the emission intensity gradually increased, and the LOD of the Rho-TTA-UNs was *ca.* 1 nM for mercury within *ca.* 5 s. Moreover, real-time tracking of the Rho-TTA-UNs was performed with the naked eye by UC in several parts of the sample. Rho-TTA-UNs were inserted into a mussel in a dish, and a few pieces of the sample were split from the mussel for PL intensity and confocal imaging after *ca.* 1 h (Fig. 7e). The split fragment on the glass was irradiated with a single-photon pulse, and mercury was monitored by DC PL.

Conclusions

In this study, dual-conversion PL nanohybrids, Rho-TTA-UNs, were first proposed as a distinctive advanced detection and tracking technology compared to other optical detection methodologies in the applications of *in vitro* and *in vivo* diagnosis. Conventional PL analysis requires more than two excitation sources for detection and tracking, while these nanohybrids enable the realization of both functions with a single-photon-driven UC/DC system. The Rho-TTA-UNs showed two different emissions under a single-photon pulse: (i) upconversion from the TTA-UC nanocapsules for tracking and (ii) downconversion from Rho-Hz for mercury ion detection *via* a turn-on system. Their performances were demonstrated by PL measurements and showed increasing PL intensity as the mercury ion solution concentration increased. The reaction time between Rho-Hz and mercury was very fast (*ca.* 5 s). Moreover, the Rho-TTA-UNs were applied for *in vivo* testing in mussels and showed high-performance mercury detection and real-time tracking. Based on these results, our new materials with UC/DC driven by a single photon can offer a new methodology for replacing indicators and probes in the field of diagnosis.[41]

Author contributions

S. S. E., C. S. P., S. J. P., S. H. L., H. S. S. and T. H. H. conducted the experiments and wrote the manuscript. K. K. H., J.-H. K., H. W. Y. and J.-Y. L. contributed to data collection and theoretical interpretation. H.-I. K. and O. S. K. designed and supervised the project and wrote the manuscript. All authors reviewed the manuscript.

Conflicts of interest

There are no conflicts to declare.

Acknowledgements

This work was supported by the Brain Research Program through the National Research Foundation (NRF) of Korea government (MSIT) (NRF-2016M3C7A1905384); a Technology Program for establishing biocide safety management from the Korea Environmental Industry & Technology Institute, funded by the Korea Ministry of Environment (no. RE201804085); the BioNano Health-Guard Research Center funded by the MSIT of Korea as a Global Frontier Project (HGUARD_2013-M3A6B2078950); the National Research Foundation of Korea (NRF) Grant funded by the Ministry of Science and ICT for the First-Mover Program for Accelerating Disruptive Technology Development (NRF-2018M3C1B9069834); the National Research Foundation of Korea (NRF) Grant funded by the Ministry of Science and ICT (NRF-2019M3C1B8077544); the Korea Electric Power Corporation (R18XA06-29); the Korea Institute of Planning and Evaluation for Technology in Food, Agriculture and Forestry (IPET) through the Advanced Production Technology Development Program, funded by the Ministry of Agriculture, Food and Rural Affairs (MAFRA) (318104-3) and the KRIBB Initiative Research Program.

Notes and references

1 W. Wang, X. Li, X. Hou, S. Wang, F. Wang and X. Luo, *ChemistrySelect*, 2017, **2**, 11880–11885.
2 R. Zhang and W. Chen, *Biosens. Bioelectron.*, 2014, **55**, 83–90.
3 A. Fang, H. Chen, H. Li, M. Liu, Y. Zhang and S. Yao, *Biosens. Bioelectron.*, 2017, **87**, 545–551.
4 Y. Zhao, S. S. You, A. Zhang, J. H. Lee, J. Huang and C. M. Lieber, *Nat. Nanotechnol.*, 2019, **14**, 783–790.
5 M. An, J. Cui, Q. He and L. Wang, *J. Mater. Chem. B*, 2013, **1**, 1333–1339.

6 A. Salinas-Castillo, M. Ariza-Avidad, C. Pritz, M. Camprubi-Robles, B. Fernandez, M. J. Ruedas-Rama, A. Megia-Fernandez, A. Lapresta-Fernandez, F. Santoyo-Gonzalez, A. Schrott-Fischer and L. F. Capitan-Vallvey, *Chem. Commun.*, 2013, **49**, 1103–1105.
7 C. Wohnhaas, A. Turshatov, V. Mailander, S. Lorenz, S. Baluschev, T. Miteva and K. Landfester, *Macromol. Biosci.*, 2011, **11**, 772–778.
8 C. Wohnhaas, V. Mailander, M. Droge, M. A. Filatov, D. Busko, Y. Avlasevich, S. Baluschev, T. Miteva, K. Landfester and A. Turshatov, *Macromol. Biosci.*, 2013, **13**, 1422–1430.
9 F. Wang, R. Deng, J. Wang, Q. Wang, Y. Han, H. Zhu, X. Chen and X. Liu, *Nat. Mater.*, 2011, **10**, 968–973.
10 K. Borjesson, P. Rudquist, V. Gray and K. Moth-Poulsen, *Nat. Commun.*, 2016, **7**, 12689.
11 R. Deng, X. Xie, M. Vendrell, Y. T. Chang and X. Liu, *J. Am. Chem. Soc.*, 2011, **133**, 20168–20171.
12 M. Kumar and P. Zhang, *Biosens. Bioelectron.*, 2010, **25**, 2431–2435.
13 B. Zhou, B. Shi, D. Jin and X. Liu, *Nat. Nanotechnol.*, 2015, **10**, 924–936.
14 X. Zhu, W. Feng, J. Chang, Y. W. Tan, J. Li, M. Chen, Y. Sun and F. Li, *Nat. Commun.*, 2016, **7**, 10437.
15 B. Zheng, H. Wang, H. Pan, C. Liang, W. Ji, L. Zhao, H. Chen, X. Gong, X. Wu and J. Chang, *ACS Nano*, 2017, **11**, 11898–11907.
16 H.-i. Kim, O. S. Kwon, S. Kim, W. Choi and J.-H. Kim, *Energy Environ. Sci.*, 2016, **9**, 1063–1073.
17 O. S. Kwon, H. S. Song, J. Conde, H. I. Kim, N. Artzi and J. H. Kim, *ACS Nano*, 2016, **10**, 1512–1521.
18 O. S. Kwon, J. H. Kim, J. K. Cho and J. H. Kim, *ACS Appl. Mater. Interfaces*, 2015, **7**, 318–325.
19 Y. Zhang, L. Wu, Y. Tang, Y. Su and Y. Lv, *Anal. Methods*, 2014, **6**, 9073–9077.
20 E. M. Nolan and S. J. Lippard, *J. Am. Chem. Soc.*, 2003, **125**, 14270–14271.
21 W. Lu, X. Qin, S. Liu, G. Chang, Y. Zhang, Y. Luo, A. M. Asiri, A. O. Al-Youbi and X. Sun, *Anal. Chem.*, 2012, **84**, 5351–5357.
22 Z. Gu, M. Zhao, Y. Sheng, L. A. Bentolila and Y. Tang, *Anal. Chem.*, 2011, **83**, 2324–2329.
23 E. M. Nolan and S. J. Lippard, *J. Am. Chem. Soc.*, 2007, **129**, 5910–5918.
24 Z. Sun, K. Cheng, Y. Yao, F. Wu, J. Fung, H. Chen, X. Ma, Y. Tu, L. Xing, L. Xia and Z. Cheng, *ACS Nano*, 2019, **13**, 1153–1167.
25 M. H. Lee, J. S. Wu, J. W. Lee, J. H. Jung and J. S. Kim, *Org. Lett.*, 2007, **9**, 2501–2504.
26 Z. Yang, Y. Zhao, S. Chen, Y. Bu, X. Zhu, Y. Du and F. Li, *Sens. Actuators, B*, 2016, **235**, 414–419.
27 L.-J. Tian, Y. Min, X.-M. Wang, J.-J. Chen, W.-W. Li, J.-Y. Ma and H.-Q. Yu, *ACS Appl. Bio Mater.*, 2019, **2**, 2661–2667.
28 K. Bera, A. K. Das, M. Nag and S. Basak, *Anal. Chem.*, 2014, **86**, 2740–2746.
29 S. Gu, C.-T. Hsieh, Y.-Y. Tsai, Y. Ashraf Gandomi, S. Yeom, K. D. Kihm, C.-C. Fu and R.-S. Juang, *ACS Appl. Nano Mater.*, 2019, **2**, 790–798.
30 A. Monguzzi, R. Tubino and F. Meinardi, *Phys. Rev. B: Condens. Matter Mater. Phys.*, 2008, **77**, 155122.
31 J. Zhao, S. Ji and H. Guo, *RSC Adv.*, 2011, **1**, 937–950.
32 A. K. Bansal, W. Holzer, A. Penzkofer and T. Tsuboi, *Chem. Phys.*, 2006, **330**, 118–129.
33 S. Akbari, T. Pirbodaghi, R. D. Kamm and P. T. Hammond, *Lab Chip*, 2017, **17**, 2067–2075.
34 M. A. Quadir, S. W. Morton, L. B. Mensah, K. Shopsowitz, J. Dobbelaar, N. Effenberger and P. T. Hammond, *Nanomedicine*, 2017, **13**, 1797–1808.
35 Z. Yang, S. Chen, Y. Zhao, P. Zhou and Z. Cheng, *Sens. Actuators, B*, 2018, **266**, 422–428.
36 J. Kuchlyan, S. Basak, D. Dutta, A. K. Das, D. Mal and N. Sarkar, *Chem. Phys. Lett.*, 2017, **673**, 84–88.
37 C. Liu, T. Xiao, Y. Wang, F. Wang and X. Chen, *Tetrahedron*, 2017, **73**, 5189–5193.
38 X.-M. Li, R.-R. Zhao, Y.-L. Wei, D. Yang, Z.-J. Zhou, J.-F. Zhang and Y. Zhou, *Chin. Chem. Lett.*, 2016, **27**, 813–816.
39 H. N. Kim, M. H. Lee, H. J. Kim, J. S. Kim and J. Yoon, *Chem. Soc. Rev.*, 2008, **37**, 1465–1472.
40 S. Hazra, C. Bodhak, S. Chowdhury, D. Sanyal, S. Mandal, K. Chattopadhyay and A. Pramanik, *Anal. Bioanal. Chem.*, 2019, **411**, 1143–1157.
41 F. C. Lam, S. W. Morton, J. Wyckoff, T. L. Vu Han, M. K. Hwang, A. Maffa, E. Balkanska-Sinclair, M. B. Yaffe, S. R. Floyd and P. T. Hammond, *Nat. Commun.*, 2018, **9**, 1991.
42 A. Leite, A. M. Silva, L. Cunha-Silva, B. de Castro, P. Gameiro and M. Rangel, *Dalton Trans.*, 2013, **42**, 6110–6118.
43 S. H. Askes, A. Bahreman and S. Bonnet, *Angew. Chem., Int. Ed. Engl.*, 2014, **53**, 1029–1033.
44 S. Mattiello, A. Monguzzi, J. Pedrini, M. Sassi, C. Villa, Y. Torrente, R. Marotta, F. Meinardi and L. Beverina, *Adv. Funct. Mater.*, 2016, **26**, 8447–8454.
45 S. H. Askes, W. Pomp, S. L. Hopkins, A. Kros, S. Wu, T. Schmidt and S. Bonnet, *Small*, 2016, **12**, 5579–5590.
46 M. Pandurangappa and K. S. Kumar, *Anal. Methods*, 2011, **3**, 715.
47 D. Jiang, X. Xue, G. Zhang, Y. Wang, H. Zhang, C. Feng, Z. Wang and H. Zhao, *J. Mater. Chem. C*, 2019, **7**, 3576–3589.